CHEMICAL ENGINEERING TRANSACTIONS
VOL. 102, 2023
A publication of AIDIC
The Italian Association of Chemical Engineering
Online at www.cetjournal.it
Guest Editors: Laura Piazza, Mauro Moresi, Francesco Donsì

ISBN 979-12-81206-01-4; **ISSN** 2283-9216
DOI: 10.3303/CET23102019

Photocatalytic Activity of Composites for Ethylene Degradation under UV-A and Visible Light

Fernanda C. Fraga[a], Juan A. Cecilia[b], Enrique Rodríguez-Castellón[b], Regina F. P. M. Moreira[a,*]

[a]Laboratory of Energy and Evironment (LEMA), Department os Chemical and Food Engineering, Federal University of Santa Catarina (UFSC), 88040-900 Florianópolis, SC, Brazil
[b]Department of Inorganic Chemistry, Faculty of Sciences, University of Malaga, 29071 Málaga, Spain
regina.moreira@ufsc.br

Ethylene is a natural hormone responsible for many processes, including ripening. One way to extend the shelf life of several fruits and vegetables is to remove ethylene from the atmosphere of storage and transport, for which photocatalysis processes can be an efficient technology. In this study, we investigated the ethylene photodegradation of four different composites (Cu/C_3N_4, Cu/TiO_2, Ni/C_3N_4, Ni/TiO_2) under UV-A and visible illumination. The photocatalytic composites were characterized, and the photocatalytic assay was performed in a continuous system for 1 h (ethylene concentration at 1.0 % in synthetic air, 50 $mL.min^{-1}$, and 400 mg of photocatalyst). The results indicated that the Cu/C_3N_4 sample did not produce carbon dioxide under visible light or UV-A illumination, so ethylene was not degraded. The Ni/TiO_2 sample had the best performance for ethylene degradation under visible light and UV-A illumination, showing higher CO_2 production with UV-A. After illumination for 1 h, the light was turned off, and 5 min later, the CO_2 concentration at the outlet was equal to the initial. Thus, the composites Ni/C_3N_4, Cu/TiO_2, and Ni/TiO_2 proved to be efficient in ethylene degradation. Therefore, they can increase the shelf life of fruits and vegetables, using photocatalysis to remove ethylene from the atmosphere while storing and transporting these foods.

1. Introduction

Ethylene is a vegetal hormone responsible for many processes, including ripening, and in climacteric fruits, the effects of this compound are pronounced (Gaikwad et al., 2020). During transport and storage of these fruits, ripening is accelerated due to ethylene. Therefore, its removal from the atmosphere is crucial to increase the post-harvest storage time of climacteric fruits (Hu et al., 2019). On the other hand, it can be used as a fruit ripening stimulator (Hu et al., 2019). For that, it is necessary to modulate the ethylene concentration, and different techniques have been applied for the removal and oxidation of ethylene, such as adsorption (Tirgar et al., 2018), chemical oxidation (Hernando et al., 2019), reduction temperature and modified atmosphere (Phakdee and Chaiprasart, 2020). Besides that, photocatalytic ethylene degradation can increase the shelf life of climacteric fruits (Fonseca et al., 2021).
Titanium dioxide is the most used photocatalyst due to its advantages: physical and chemical stability, photostability, low toxicity, optical activity, and cost-effectiveness (Etacheri et al., 2015; Verbruggen, 2015). The TiO_2 for ethylene degradation is well known, and its degradation mechanisms are proposed by Hauchecorne et al. (2011). However, the absorption range limits the application with the use of UV light due to its band gap energy (~ 3.2 eV) (Kitano et al., 2016). Nevertheless, titanium dioxide modification by metal or non-metallic doping, for example, can produce visible-light responsive photocatalysts (Baruah et al., 2022).
The semiconductor carbon nitride (C_3N_4) has gained prominence in several reports as a photocatalyst due to the light absorption in the visible range, with about 2.7 eV as optical band gap energy. Moreover, carbon nitride has chemical and thermal stability, low cost, good electrical properties, and can quickly be produced from urea, melamine, or other organic nitrogen sources (Qi et al., 2020). However, the electron-hole recombination rate is high when used pure, so the photocatalytic activity is relatively low (Qi et al., 2020). Metal doping can be

Paper Received: 8 March 2023; Revised: 28 April 2023; Accepted: 1 September 2023
Please cite this article as: Fraga F.C., Cecilia J.A., Rodriguez-Castellon E., Moreira R.F., 2023, Photocatalytic Activity of Composites for Ethylene Degradation Under UV-A and Visible Light, Chemical Engineering Transactions, 102, 109-114 DOI:10.3303/CET23102019

promoted advantages like as: separation and transfer of charge efficiency, decrease in the band gap energy, visible light absorption, and reduction charge recombination for g-C_3N_4 (Díaz et al., 2021).
Considering the g-C_3N_4 and TiO_2 characteristics useful in the photocatalysis field, doping with transition metals, such as nickel and copper, can result in high photocatalytic activity under visible light and a low recombination rate, as reported by Muñoz-Batista et al. (2020) and Díaz et al. (2021). As nickel and titanium atoms have similar ionic radii, 0.72 and 0.68 Å, respectively, it is possible to introduce Ni atoms in the structure of TiO_2 (Baruah et al., 2022).
In this work, we investigated ethylene degradation using copper, nickel, titanium dioxide, and carbon nitride composites. For that, photocatalytic composites (Cu/C_3N_4, Cu/TiO_2, Ni/C_3N_4, Ni/TiO_2) were characterized by X-ray Diffraction (XRD), surface area and pore volume by nitrogen adsorption/desorption, scanning electron microscopy (FEG-SEM) coupled with an energy dispersive spectrometer, diffuse reflectance (DRS) and X-ray photoelectron (XPS) spectroscopy.

2. Experimental details

The photocatalytic composites with 5 % (% wt) Cu or Ni, denominated Cu/C_3N_4, Cu/TiO_2, Ni/C_3N_4, Ni/TiO_2, were synthesized and characterized in previous work (Díaz et al., 2021). Morphologies were investigated by scanning electron microscopy (FEG-SEM, model JEOL JSM-6701F) coupled with an energy dispersive spectrometer (EDS), the nitrogen adsorption/desorption isotherm measurements were performed (MicroActive 5.02, micromeritics®) and the specific surface area and the pore volume were characterized by Brunauer-Emmett-Teller (BET). X-ray diffraction (XDR) (Rigaku Miniflex II) with CuKα radiation (1.5406 Å) was used by crystallite structures investigation under the following conditions: 15 mA electric current and 30 kV potential difference ($10 < \theta < 90$ °). Scherrer's equation was utilized for crystallite size τ estimation: with Bragg's angle θ (rad), form factor K = 0.9, wavelength λ = 0.15406 nm, and β = full width at half maximum peak (FWHM) (Scherrer, 1912). Optical proprieties were determined by Kubelka-Munk, through diffuse reflectance spectroscopy (DRS, UV-Vis/NIR Cary 7000, Agilent) using $BaSO_4$ and band gap estimated by Tauc's plot (Tauc, 1968). X-ray photoelectron spectroscopy (XPS) spectra were obtained (Physical Electronics PHI 5700, Al-Kα radiation), and adventitious carbon (C 1*s* at 284.8 eV) was used as reference, the deconvolution curves were fitted using Gaussian-Lorentzian model in Multipak software.
The photocatalytic assay was performed in a previously described system and adapted analysis conditions (Fraga et al., 2022), with inlet ethylene concentration at 1.0 % (mol/mol) in synthetic air, UV-A or visible lamp (10 W) was placed on the top outside reactor (borosilicate glass semi-tubular, 100 mL volume). Photocatalyst (400 mg) was disposed onto a 26 x 76 mm glass slide, on the base of the reactor, in powder form. The flow rate (50 $mL.min^{-1}$) was kept continuous all the time. Gas samples were collected at the inlet and outlet of the reactor, injected into a gas chromatograph coupled to a mass spectrometer (GCMS, Shimadzu GC/QP 2010 Plus), monitoring the mass/ion charge ration (m/z): 44 m/z for carbon dioxide ions identification, and 27, 26 and 25 m/z for ethylene ions identification. The chromatograph operation temperature was maintained at 28 °C. The results are expressed in terms of the carbon dioxide production rate ($\mu mol.min^{-1}.g_{cat}^{-1}$).

3. Results and discussion

3.1 Structural, textual, and chemical characterization

XRD patterns of all samples are shown in Figure 1. Samples containing TiO_2 (Figure 1a) showed peaks characteristic of the anatase phase at: 25.3, 38,7, 48.0, 53.9, 55.4, 62.8, 68.7, 70.4, and 75.3 °, related to the (1 0 1), (1 1 2), (2 0 0), (1 0 5), (2 1 1), (2 0 4), (1 1 6), (2 2 0), and (2 1 5) planes, respectively (JCPDS cars nº 00-021-1272). However, characteristic peaks of the rutile phase were also observed at: 27.4, 35.3, 41.3, 44.4, 56.7, and 82.8 °. These peaks were expected, and similar results having diffraction peaks for TiO_2 were reported in the literature (Baruah et al., 2022). In addition, weak peaks around 17.5 and 21.5 ° could be ascribed to the presence of Cu (Zhang et al., 2022). However, the presence of these metals (Ni or Cu) was not detected clearly, due to the small percentage of Ni or Cu in the samples, being the relative intensity of the peaks of TiO_2 higher than that of Ni or Cu. The peak around at 12.9 ° present in samples containing C_3N_4 (Figure 1b) is identified as the (1 0 1) plane of graphitic carbon nitride (g-C_3N_4), and the 27.5 ° peak is related to the (0 0 2) plane, associated to the stacking between layers of conjugated aromatic of the graphitic materials (Muñoz-Batista et al., 2020). Peaks observed around 43.5 º are related to the metallic form of Cu or Ni (Fernández-Catalá et al., 2021; Sharma et al., 2021). The value of the crystallite sizes calculated were: 16.1, 15.0, 7.5, and 7.6 nm, for Ni/TiO_2, Cu/TiO_2, Ni/C_3N_4, and Cu/C_3N_4, respectively. Similar values are reported in the literature (Baruah et al., 2022; Fernández-Catalá et al., 2021).

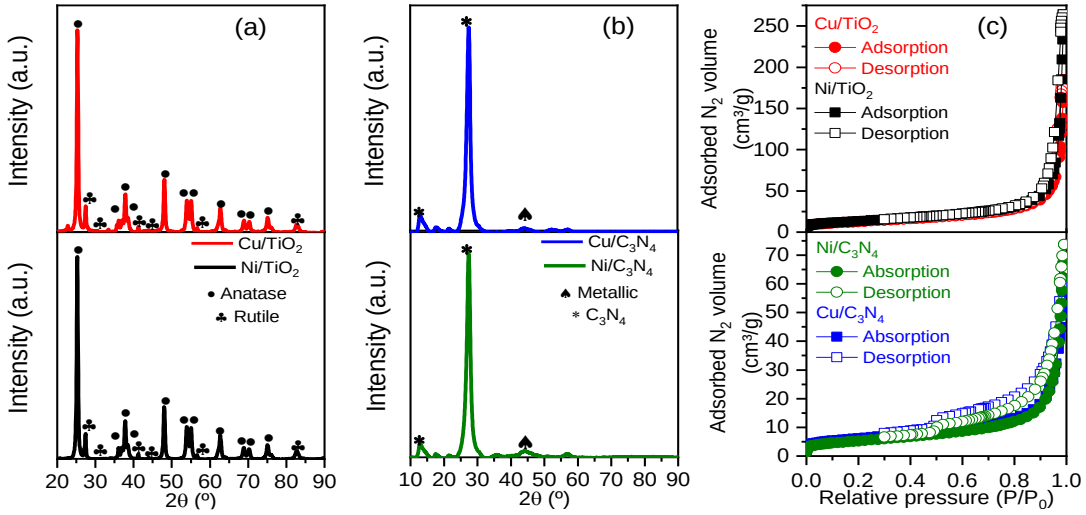

Figure 1: X-ray diffractogram of samples Cu/TiO_2 and Ni/TiO_2 (a), Cu/C_3N_4 and Ni/C_3N_4 (b) and N_2 adsorption-desorption isotherms (c)

The nitrogen adsorption-desorption isotherms were indicated in Figure 1c, it is possible to observe that all samples have type III isotherms, indicated surface of a macropores solids, the type H3 hysteresis indicated that the macropores which are not entirely filled (Thommes et al., 2015). The surface area obtained by BET analysis indicated TiO_2 compounds have a higher surface area than C_3N_4 compounds, and the average pore diameter for Cu-doped catalysts were like each other. Similar behavior was observed for Ni-doped catalysts, and the higher total pore volume was observed for the Ni/TiO_2 sample. Then, it could be expected that Ni-doped catalysts have a higher catalytic activity since the number the active sites would be higher than for Cu-doped catalysts. These results were summarized in Table 1.

Table 1: Surface characterization, particle size, chemical composition, and carbon dioxide production rate of the samples

Sample	BET surface area ($m^2.g^{-1}$)	Average pore diameter (Å)	Total pore volume ($cm^3.g^{-1}$)	Average particles size (µm)	Elemental analysis from EDS (wt, %)						Rate VIS (µmol. $min^{-1}.g_{cat}^{-1}$)	Rate UV-A (µmol. $min^{-1}.g_{cat}^{-1}$)
					C	N	Ni	Cu	Ti	O		
Cu/TiO_2	44	77.4	0.086	3.58	-	-	-	4.2	52.4	43.3	0.0029 ± 0.0005	0.056 ± 0.002
Ni/TiO_2	48	90.6	0.108	4.30	-	-	0	-	53.3	46.7	0.0070 ± 0.0010	0.310 ± 0.010
Cu/C_3N_4	22	76.4	0.041	2.41	40.1	59.9	-	0	-	-	-	-
Ni/C_3N_4	19	86.1	0.040	2.05	36.6	63.4	0	-	-	-	0.0010 ± 0.0008	0.004 ± 0.001

Figure 2 shows that heterogeneous and agglomerated particles with micrometric sizes (Table 1) can be observed from the FEG-SEM analysis. The average value was evaluated by measuring approximately 100 particles for each sample using open-source ImageJ software (Pascariu et al., 2022). The chemical compositions obtained by EDS and the measurement results are presented in Table 1. It is noted that no other impurities were presented. Micrometer agglomerate of TiO_2 can be identified from the FEG-SEM (Figure 2a and Figure 2b). The composition of the Cu/TiO_2 sample obtained by EDS is very close to the theoretical value. Though, Ni was not detected in both samples. Microsheets structures are observed in samples that have C_3N_4 in their composition (Figure 2c and Figure 2d), being a characteristic of this compound. The molar ratio C:N is nearly equal to the theoretically expected. However, Ni or Cu was not detected by EDS in the C_3N_4 presence, and as can be seen from the XRS results, the relative peaks confirm that the percentage of nickel or copper was very small.

Absorbance spectrums of the samples are presented in Figure 2e, and all the photocatalysts synthesized absorb in the visible light range. The band gap energies were estimated by Kubelka-Munk function and Tauc's plot: $(F(R)h\nu)^{2/n}$ *versus* Energy (eV), considering indirect allowed transition (n = 4) for TiO_2 samples (López and Gómez, 2012) and direct transition (n = 1) for C_3N_4 composites (Huo et al., 2018), as shown in Figure 2f. The obtained band gap energy (E_g) values were: 2.74 (dashed red line), 2.94 (dashed black line), 2.84 (dashed blue

line), and 2.63 eV (dashed green line) for Cu/TiO_2, Ni/TiO_2, Cu/C_3N_4, and Ni/C_3N_4, respectively. These results show a reduction in the band gap energy due to the use of metals (copper and nickel), compared to pure TiO_2, whose value is around 3.2 eV (López and Gómez, 2012). Furthermore, these results suggests that these composites have activation under visible light (E_g < 3.11 eV).

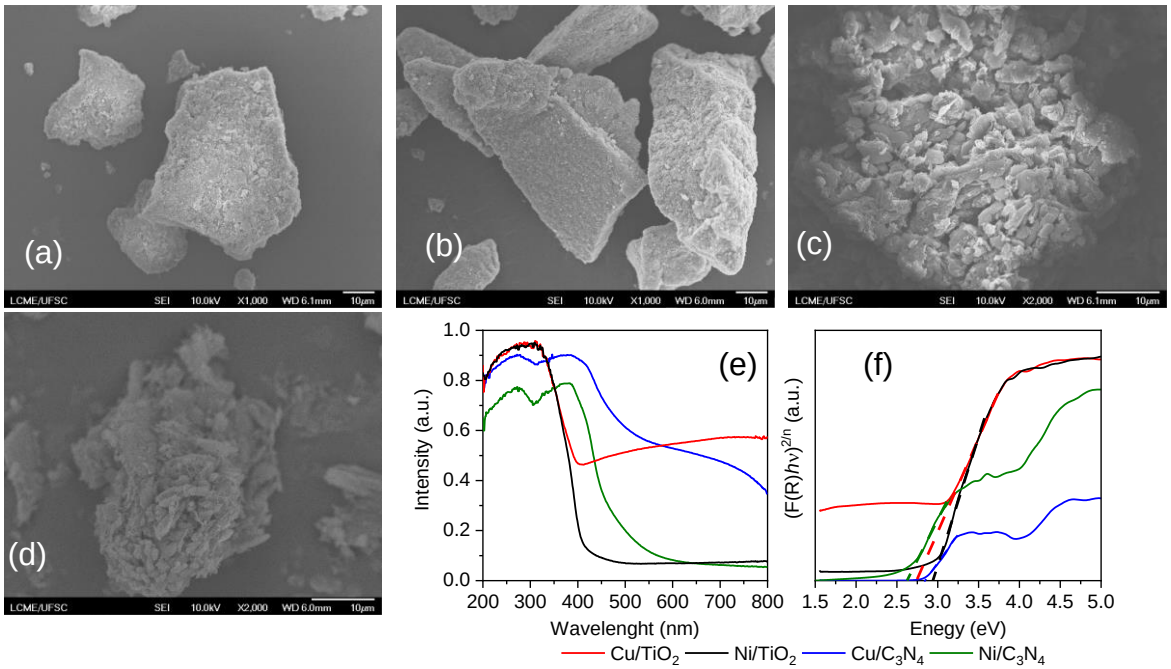

Figure 2: FEG-SEM images of Cu/TiO_2 (a), Ni/TiO_2 (b), Cu/C_3N_4 (c), and Ni/C_3N_4 (d), absorbance spectrum (e) and Tauc's plot (f) of the samples

Figure 3a displays the C 1*s* XPS peak, and all samples have contributions from the C-C and C-OH signals. C_3N_4 samples have a peak related to aromatic rings (N-C=N), confirmed from N 1*s* XPS spectrum (Figure 3b), where was identified a peak corresponding to graphitic nitrogen (Zhang et al., 2022). The Cu 2*p* XPS spectra (Figure 3c) show the characteristic peaks of reduced copper species (Cu^0 or Cu^+ at 932.6 eV), and Cu^{2+} at 934.2 eV in both Cu/TiO_2 and Cu/C_3N_4 photocatalysts (Fernández-Catalá et al., 2021). These results indicate that the Cu/TiO_2 sample has the existence of more stabilized reduced Cu (Cu^0 or Cu^+), while Cu/C_3N_4 sample presented more Cu^{2+}. The XPS spectra of O 1*s* (Figure 3d) have peaks at 531.6 and 529.8 eV are associated with the surface oxygen species of the hydroxyl groups and lattice oxygen of the TiO_2, respectively, confirmed in the Ti 2*p* spectra (Figure 3f), at 458.7 eV (Sharma et al., 2021). The peak around 855.6 eV in the Ni 2*p* spectra (Figure 3e) is attributed to Ni^{2+} ions (Baruah et al., 2022). The XPS results confirm the formation of the composites, and all atomic elements have been identified.

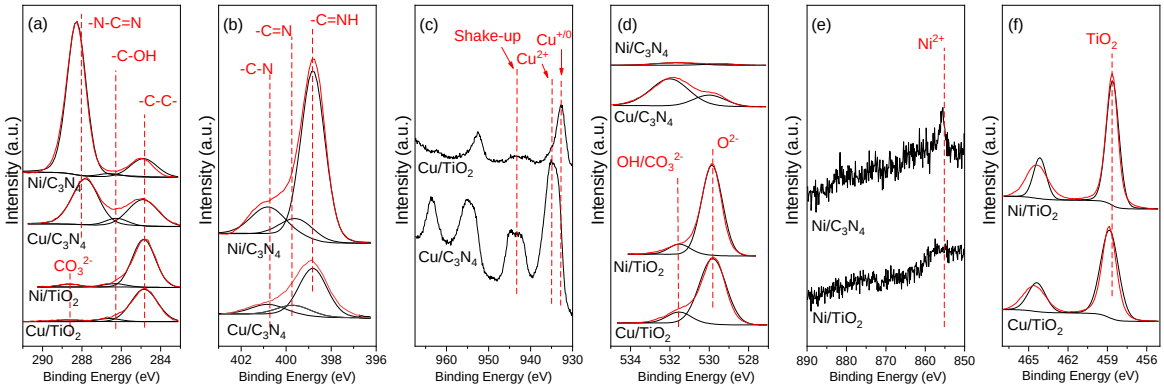

Figure 3: High-resolution XPS spectra of: C 1s (a) N 1s (b), Cu 2p (c), O 1s (d), Ni 2p (e) and Ti 2p (f) for samples. Deconvolutions into the main and satellite peaks are shown

3.2 Photocatalytic performance

The formation of CO_2 from the ethylene mineralization reactions on the outlet of the reactor was continuously measured, and the results are shown in Figure 4. The carbon dioxide production rates are summarized in Table 1. The Cu/C_3N_4 sample did not produce carbon dioxide under visible light or UV-A illumination, so ethylene was not degraded. This can be associated to the almost non-detection of copper atoms in the sample surface, the lower average pore diameter and due the fast recombination electron-hole pair of the C_3N_4.

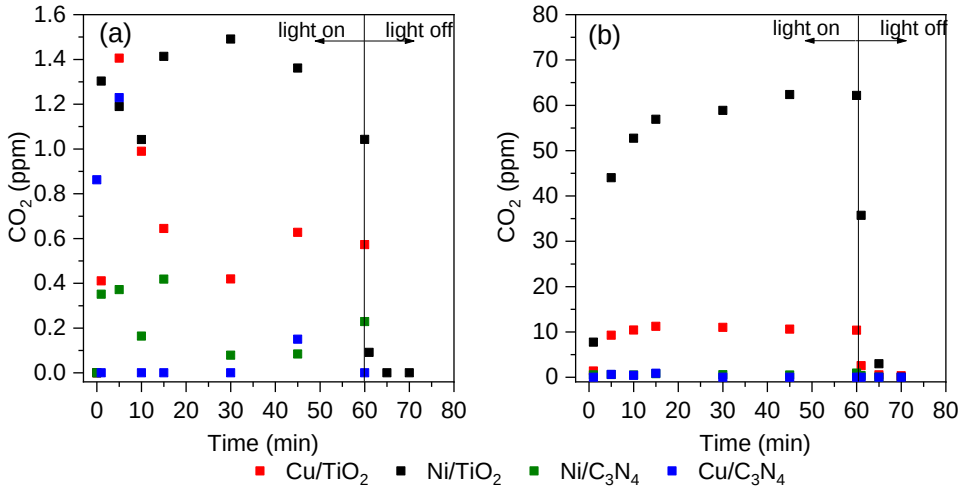

Figure 4: Carbon dioxide production concentration under visible light (a) and UV-A (b) irradiation.

The Ni/TiO_2 sample had the best performance for ethylene degradation under visible light and UV-A illumination, showing higher CO_2 production with UV-A due to the higher TiO_2 activity under this illumination and Ni presence in the sample. Besides, the metal-doping effect on photocatalytic ethylene degradation can be observed, and Ni showed higher activity than Cu when impregned in TiO_2. These results may be associated with higher surface area, average pore diameter, pore volume, and particle size than when in the presence of Cu. In addition, a lower band gap energy value was observed for Ni/TiO_2 than for Cu/TiO_2. After illumination for 1 h, the light was turned off, and 5 min later, the CO_2 concentration at the outlet was equal to the initial value, proving the photocatalysis process. Thus, the composites Ni/C_3N_4, Cu/TiO_2, and Ni/TiO_2 proved efficient in ethylene degradation. Therefore, they can be used to increase the shelf life of fruits and vegetables, using photocatalysis to remove ethylene from the atmosphere during the storage and transport of these foods.

4. Conclusions

The 5 %-metal (nickel and copper)- doped in TiO_2 or C_3N_4 were characterized, and crystalline compounds were found. SEM images of the particles have confirmed the presence of heterogeneous particle agglomerates in micrometric particle size and microsheet structure in metal doped-TiO_2 or -C_3N_4, respectively. The EDS analysis indicated the presence of Cu in one sample (Cu/TiO_2) with a percentage close to the theoretical. The XPS results confirm the presence of all atomic elements in the samples. The Ni-doped TiO_2 sample presented the highest photocatalytic activity under UV and visible light irradiation. Textural parameters (surface area, average pore diameter, pore volume) and particle size positively affected Ni-doped TiO_2 samples' photoactivity.

Acknowledgments

This study was financed in part by the Coordenação de Aperfeiçoamento de Pessoas de Nível Superior – Finance Code 001. The authors thank LCME/UFSC and LINDEN/UFSC laboratories for the characterization analysis. J.A.C. and E.R.C. thanks to Ministerio de Ciencia e Innovación of Spain, Grant PID2021-126235OB-C32.

References

Baruah, M., Ezung, S.L., Sharma, S., Sinha, U.B., Sinha, D., 2022, Synthesis and characterization of Ni-doped TiO2 activated carbon nanocomposite for the photocatalytic degradation of anthracene, Inorg. Chem. Commun., 144, 109905.

Díaz, L., Rodríguez, V.D., González-Rodríguez, M., Rodríguez-Castellón, E., Algarra, M., Núñez, P., Moretti, E., 2021, M/TiO2 (M = Fe, Co, Ni, Cu, Zn) catalysts for photocatalytic hydrogen production under UV and visible light irradiation, Inorg. Chem. Front., 8, 3491–3500.

Etacheri, V., Di Valentin, C., Schneider, J., Bahnemann, D., Pillai, S.C., 2015, Visible-light activation of TiO2 photocatalysts: Advances in theory and experiments, J. Photochem. Photobiol. C Photochem. Rev., 25, 1–29.

Fernández-Catalá, J., Navlani-García, M., Verma, P., Berenguer-Murcia, Á., Mori, K., Kuwahara, Y., Yamashita, H., Cazorla-Amorós, D., 2021, Photocatalytically-driven H2 production over Cu/TiO2 catalysts decorated with multi-walled carbon nanotubes, Catal. Today, 364, 182–189.

Fonseca, J. de M., Pabón, N.Y.L., Nandi, L.G., Valencia, G.A., Moreira, R. de F.P.M., Monteiro, A.R., 2021, Gelatin-TiO2-coated expanded polyethylene foam nets as ethylene scavengers for fruit postharvest application, Postharvest Biol. Technol., 180, 111602.

Fraga, F.C., Della Rocca, D.G., José, H.J., Victória, H.F.V., Gabriel Filho, J.B., Krambrock, K., Rodríguez-Castellón, E., Moreira, R. de F.P.M., 2022, Evaluation of reactive oxygen species and photocatalytic degradation of ethylene using β-Ag2MoO4/g-C3N4 composites, J. Photochem. Photobiol. A Chem., 432, 114102.

Gaikwad, K.K., Singh, S., Negi, Y.S., 2020, Ethylene scavengers for active packaging of fresh food produce, Environ. Chem. Lett., 18, 269–284.

Hauchecorne, B., Tytgat, T., Verbruggen, S.W., Hauchecorne, D., Terrens, D., Smits, M., Vinken, K., Lenaerts, S., 2011, Photocatalytic degradation of ethylene: An FTIR in situ study under atmospheric conditions, Appl. Catal. B Environ., 105, 111–116.

Hernando, A., Ariyanto, T., Prasetyo, I., 2019, Preserving climacteric fruits by ripening hormone oxidation using nano-KMnO4 confined within nanoporous carbon, ASEAN J. Chem. Eng., 19, 54–65.

Hu, B., Sun, D.-W., Pu, H., Wei, Q., 2019, Recent advances in detecting and regulating ethylene concentrations for shelf-life extension and maturity control of fruit: A review, Trends Food Sci. Technol., 91, 66–82.

Huo, Y., Wang, Z., Zhang, J., Liang, C., Dai, K., 2018, Ag SPR-promoted 2D porous g-C3N4/Ag2MoO4 composites for enhanced photocatalytic performance towards methylene blue degradation, Appl. Surf. Sci., 459, 271–280.

Kitano, S., Tanaka, A., Hashimoto, K., Kominami, H., 2016, Metal ion-modified TiO2 photocatalysts having controllable oxidative performance under irradiation of visible light, Appl. Catal. A Gen., 521, 202–207.

López, R., Gómez, R., 2012, Band-gap energy estimation from diffuse reflectance measurements on sol-gel and commercial TiO2: A comparative study, J. Sol-Gel Sci. Technol., 61, 1–7.

Muñoz-Batista, M.J., Andrini, L., Requejo, F.G., Gómez-Cerezo, M.N., Fernández-García, M., Kubacka, A., 2020, Sunlight active g-C3N4-based Mn+ (M = Cu, Ni, Zn, Mn) – promoted catalysts: Sharing of nitrogen atoms as a door for optimizing photo-activity, Mol. Catal., 484, 110725.

Pascariu, P., Cojocaru, C., Samoila, P., Airinei, A., Olaru, N., Rotaru, A., Romanitan, C., Tudoran, L.B., Suchea, M., 2022, Cu/TiO2 composite nanofibers with improved photocatalytic performance under UV and UV–visible light irradiation, Surfaces and Interfaces, 28, 101644.

Phakdee, N., Chaiprasart, P., 2020, Modified atmosphere storage extends the shelf life of ‘Nam Dok Mai Sri Tong’ mango fruit, Int. J. Fruit Sci., 20, 495–505.

Qi, K., Liu, S., Zada, A., 2020, Graphitic carbon nitride, a polymer photocatalyst, J. Taiwan Inst. Chem. Eng., 109, 111–123.

Scherrer, P., 1912, Bestimmung der inneren Struktur und der Größe von Kolloidteilchen mittels Röntgenstrahlen. In: Kolloidchemie Ein Lehrbuch, Springer Berlin Heidelberg, Berlin, Heidelberg, pp. 387–409.

Sharma, S.K., Banerjee, A., Paul, B., Poddar, M.K., Sasaki, T., Samanta, C., Bal, R., 2021, Combined experimental and computational study to unravel the factors of the Cu/TiO2 catalyst for CO2 hydrogenation to methanol, J. CO2 Util., 50, 101576.

Tauc, J., 1968, Optical properties and electronic structure of amorphous Ge and Si, Mater. Res. Bull., 3, 37–46.

Thommes, M., Kaneko, K., Neimark, A. V., Olivier, J.P., Rodriguez-Reinoso, F., Rouquerol, J., Sing, K.S.W., 2015, Physisorption of gases, with special reference to the evaluation of surface area and pore size distribution (IUPAC Technical Report), Pure Appl. Chem., 87, 1051–1069.

Tirgar, A., Han, D., Steckl, A.J., 2018, Absorption of ethylene on membranes containing potassium permanganate loaded into alumina-nanoparticle-incorporated alumina/carbon nanofibers, J. Agric. Food Chem., 66, 5635–5643.

Verbruggen, S.W., 2015, TiO2 photocatalysis for the degradation of pollutants in gas phase: From morphological design to plasmonic enhancement, J. Photochem. Photobiol. C Photochem. Rev., 24, 64–82.

Zhang, X., Zhang, X.R., Yang, P., Chen, H.-S., Jiang, S.P., 2022, Black magnetic Cu-g-C3N4 nanosheets towards efficient photocatalytic H2 generation and CO2/benzene conversion, Chem. Eng. J., 450, 138030.